SCIENTIFIC PAPER
Published: May 5, 2025
https://doi.org/10.13167/2025.30.11

Investigating the feasibility of utilising bagasse ash and reclaimed asphalt pavement dust in geopolymer mortar

Sajan Sharma[1] and Shailja Bawa[1]

[1] D.R. B.R Ambedkar National Institute of Technology, Research Scholar, Department of Civil Engineering, Jalandhar, Punjab 144011, India

Corresponding author:
Sajan Sharma
sajans.ce.22@nitj.ac.in

Received:
September 20, 2024

Revised:
March 30, 2025

Accepted:
April 1, 2024

Published:
May 5, 2025

Citation:
Sharma, S.; Bawa, S. Investigating the feasibility of utilising bagasse ash and reclaimed asphalt pavement dust in geopolymer mortar. *Advances in Civil and Architectural Engineering,* 2025, 16 (30), pp. 182-206. https://doi.org/10.13167/2025.30.11

ADVANCES IN CIVIL AND ARCHITECTURAL ENGINEERING (ISSN 2975-3848)

Faculty of Civil Engineering and Architecture Osijek
Josip Juraj Strossmayer University of Osijek
Vladimira Preloga 3
31000 Osijek
CROATIA

Abstract:
Geopolymers offer a sustainable alternative by reducing environmental impacts while fulfilling construction needs. Their eco-friendly properties and performance contribute to lower CO_2 emissions and minimise landfill waste through recycling. This study investigates the properties of geopolymer mortar incorporating bagasse ash (BA) and reclaimed asphalt pavement (RAP) dust as binders in varying percentage ratios of 0; 35; 65 and 100. An activation system consisting of sodium silicate (Na_2SiO_3) and sodium hydroxide (NaOH) in ratios of 1,0; 1,5; and 2,0 with a NaOH concentration of 10 M were tested to explore the polymerisation process. A dataset of 331 samples was created for use with machine learning algorithms and served as a benchmark to compare lab-tested compressive strength. Regression analysis using random forest, gradient boost, and extreme gradient boost regressors identified the range of the R^2 value from 0,57-0,73, MAE from 7,55-23,56; and MSE from 123,45-583,75. The compressive strength (CS) of different mix designs was tested, ranging from 3,05-27,05 MPa after 28 days of testing. Thermogravimetric analysis indicated minor weight loss at specific temperature ranges, with more significant loss afterwards. Post-exposure to 1000 °C, a variation in compressive strength was noted owing to mortar matrix decomposition. The microstructural analysis identified the formation of C-A-S-H, N-A-S-H, C-S-H, and key crystallographic phases. This study provides valuable insights into optimising mixtures for targeted properties while facilitating large-scale landfill waste recovery, reducing environmental hazards, and replacing cement-based mortar, thereby contributing to sustainable construction practices.

Keywords:
geopolymer mortar; machine learning; TGA; SEM; XRD; FTIR

1 Introduction

The substantial contributions of the construction sector to carbon dioxide (CO_2) emissions, the accumulation of waste worldwide, and environmental pollution have been recognised. The urgent need to address the global impact of climate change requires researchers to pursue novel, ecologically sound, and sustainable construction materials. Geopolymer materials have emerged as promising alternatives to traditional cementitious materials and have demonstrated their potential to mitigate CO_2 emissions and reduce energy consumption in construction processes. In 1979, Davidovits introduced an innovative approach to ordinary portland cement (OPC) known as "geopolymer", characterising it as an inorganic compound. Geopolymer mortar (GPM) eliminates the need for OPC, instead relying on materials abundant in silicon (Si) and aluminium (Al), which are capable of interacting with alkaline silicates and thereby generate polymeric Si-O-Al bonds conducive to the formation of cementitious materials [1]. Geopolymers are acknowledged by the research community as environmentally sustainable materials because of their capacity for effective waste utilisation, diminished CO_2 emissions, and increased structural resilience [2]. Studies indicate that adopting geopolymers significantly mitigates CO_2 emissions, with the reductions ranging from 45-80 %, and substantially reduces energy consumption by approximately 60 % compared with conventional cementitious materials [3; 4]. Geopolymers are synthesised by amalgamating chemical alkali activators, typically sodium hydroxide (NaOH), and amorphous or semicrystalline aluminosilicates with precursors such as fly ash, slag, or red mud. Geopolymerisation is a chemical reaction between silicon (Si) and aluminium (Al) minerals in combination with an alkaline solution. This reaction leads to the formation of three-dimensional polymer chains composed of Si-O-Al-O bonds [1; 5]. The general chemical structure of geopolymer is represented by $Mn[-(SiO_2)z-Al_2O_3]\bullet wH_2O$, where z signifies the number of aluminate substitutions, n denotes the degree of geopolymerisation, M represents cation-encompassing elements such as sodium and potassium, and w indicates the water content [6; 7]. The substrate for geopolymerisation must be amorphous to facilitate chemical reactions. Greater concentrations of SiO_2, Al_2O_3, and Fe_2O_3 correspond to increased pozzolanic activity [8; 9]. Smaller precursor particles contribute to an increased specific surface area and thereby accelerate the reaction rate [10]. Geopolymer matrices surpass conventional cement matrices in various mechanical and chemical aspects, including superior compressive, flexural, and tensile strengths; enhanced fire resistance; high-temperature stability; low permeability; resistance to salt and acid; and reduced creep [5-7; 9; 10]. The characteristics of geopolymer mortar are influenced by various factors, including the origin, composition, and particle size of the precursor; concentration of the alkaline solution; curing conditions; and temperature [11]. Geopolymers exhibit exceptional thermal resilience owing to their unique three-dimensional skeletal frameworks. Studies indicate that these materials retain their inherent properties even under extreme temperatures, reaching as high as 1300 °C [5].

The compositional variability and unpredictability inherent in geopolymer mortar mixing ratios necessitate iterative experiments to determine the mechanical attributes of the resulting mixtures. These iterative trials demand significant laboratory resources, including natural materials, energy, labour, and time. Consequently, the development of a computational framework is imperative for forecasting key mechanical parameters, such as compressive strength. In recent times, there has been a surge in the utilisation of various machine learning techniques, including artificial neural networks, random forest (RF), gradient boost (GB), extreme gradient boost (XGB), and decision trees, propelled by the increasing popularity of machine learning methodologies [12-18]. The efficacy of these algorithms, as indicated by the coefficient of determination (R^2), varies depending on the specific constituents employed in the amalgamation of geopolymer mortar. In one study, an R^2 of 0.937 was obtained for slag-based geopolymers when using artificial neural networks for prediction. Another researcher achieved an R^2 value of 0,60 for fly ash combinations [19; 20]. This study revealed divergent R^2 values across various algorithms, such as XGB (0,96), RF (0.91), and ridge regression (0,53), in the context of slag mixtures, underscoring algorithmic performance disparities [21]. In this study,

a sensitivity analysis determined that the constituent material itself contributes significantly (27 %) to the strength of the resultant mixture [22]. The intricate interplay of multiple factors, such as the binder type, alkali activator type, binder/activator ratio, and curing conditions encompassing the type, duration, and temperature, engenders complex nonlinear relationships between the geopolymer matrix and its mechanical attributes, necessitating ongoing endeavours in predictive model development. In one study, a nonlinear model revealed that the compressive strengths of geopolymers derived from coal gangue and slag blends spanned a range of 20-60 MPa, contingent on the constituent proportions [23]. Another study showed that geopolymer formulations subjected to varying curing temperatures (30; 45; 75; and 90 °C) exhibited compressive strengths of more than 40 MPa [24]. Similarly, another study determined that the compressive strengths of slag and fly ash geopolymer blends varied from 8-25 MPa depending on the alkali/binder ratio [25]. To expedite the estimation of experimental data with enhanced precision, leveraging soft computing techniques and machine learning methodologies is imperative to discern mechanical attributes, such as the compressive strength of geopolymers across diverse formulations [26; 27].

The increasing emphasis on sustainable construction materials has accelerated research on geopolymer mortars, which utilise industrial byproducts and waste materials as alternative binders to conventional cement [28; 29]. Significant advancements have been made in incorporating materials such as fly ash, metakaolin, and ground granulated blast furnace slag (GGBS) [30-35]. Their large-scale adoption faces challenges owing to the commercialisation of these binders, and the declining trend in electricity production from thermal power plants can lead to the unavailability of fly ash and regional unavailability of these binder materials. Hence, exploring alternative precursors is imperative to enhancing the economic viability and broadening the applicability of geopolymers. A promising sustainable approach is the utilisation of waste materials from road construction, specifically, reclaimed asphalt pavement (RAP). RAP is a by-product obtained from asphalt pavements via milling, ripping, and crushing processes. A substantial quantity of RAP is generated annually as waste at plant sites in India [36-41]. Although extensive research has been conducted on the incorporation of RAP aggregate into conventional concrete, the potential of RAP dust as a geopolymer precursor remains largely unexplored. This study represents a significant step forward in investigating its viability as a binder material in combination with sugarcane bagasse ash (BA).

Sugarcane is a major agricultural crop globally cultivated primarily for sugar and ethanol production, with an estimated cultivation area of 31,3 million hectares. Brazil has the largest sugarcane production (36 %), and it is followed by India (17 %), Thailand (8 %), China (7 %), and Pakistan (4 %) [42]. Sugarcane processing generates sugarcane bagasse as a byproduct, which produce BA upon combustion. Studies have indicated that burning one ton of bagasse yields approximately 25-40 kg of BA. With the increasing global demand for sugar and ethanol, the generation of BA continues to increase. Research has demonstrated that BA influences the final properties of geopolymer mortars by improving their thermal resistance by up to 30 % [43; 44].

The current study aims to address the existing research gap by systematically evaluating the feasibility of RAP dust and BA as geopolymer precursor materials and investigating their performance in varying proportions. In addition, the study explores the effects of different Na_2SiO_3/NaOH ratios on the mechanical and microstructural characteristics of geopolymer mortars. Unlike conventional geopolymer research, which predominantly focuses on materials with established reactivity, this study adopted a novel approach by incorporating RAP dust, which is a waste byproduct of road maintenance activities, and validating its performance through statistical analysis, as shown in Figure 1. The hardened properties of geopolymer mortars were investigated, including the compressive strength, thermogravimetric analysis, and microstructural characterisation. Despite the potential environmental and economic benefits of RAP dust in geopolymer matrices, several practical barriers hinder its large-scale adoption in the construction industry. The key challenges include variability in material composition, potential durability concerns, and the absence of standardised guidelines for its application. The current research not only evaluates the technical performance of RAP dust

and BA-based geopolymer mortars but also discusses the fundamental obstacles that must be addressed for their practical implementation in sustainable construction.

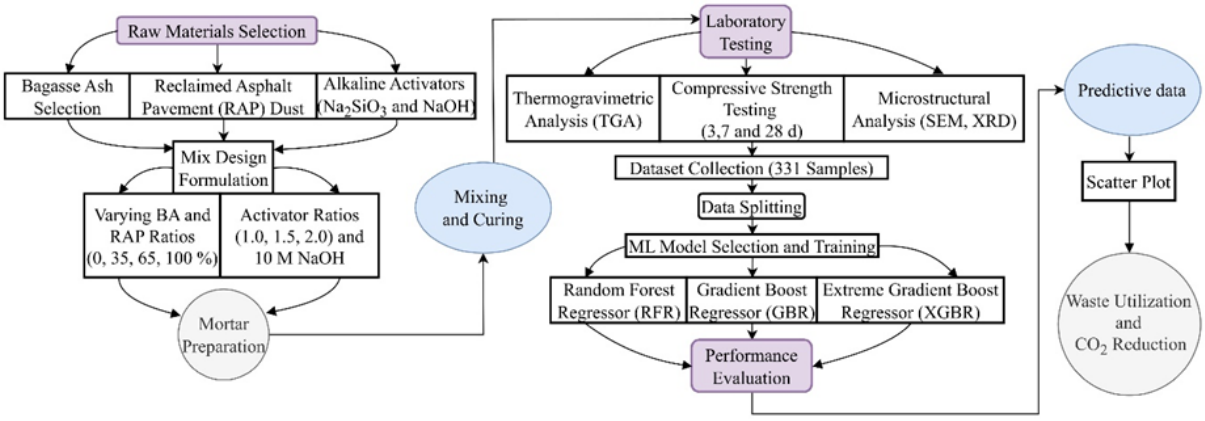

Figure 1. Schematic of geopolymer mortar formation

2 Methodology

2.1 Materials

In this study, BA was procured from the boiler of a locally accessible sugar mill situated in Phagwara, Punjab, India. Prior to utilisation, the bagasse ash underwent a process of refinement, wherein it was finely ground using a ball mill and subsequently sieved through a 75 µm sieve to achieve uniform particle size distribution. The specific gravity of BA was determined to be 1,29; with an observed SiO_2/Al_2O_3 ratio of 1,47; providing insights into its compositional characteristics. Concurrently, the RAP material utilised in this study was sourced locally and subjected to similar processing procedures. Following milling and sieving through a 75 µm sieve, the resulting RAP dust, as a novel material for geopolymer mortar, exhibited a specific gravity of 2,34 along with a SiO_2/Al_2O_3 ratio of 3,16; as depicted in Figure 2.

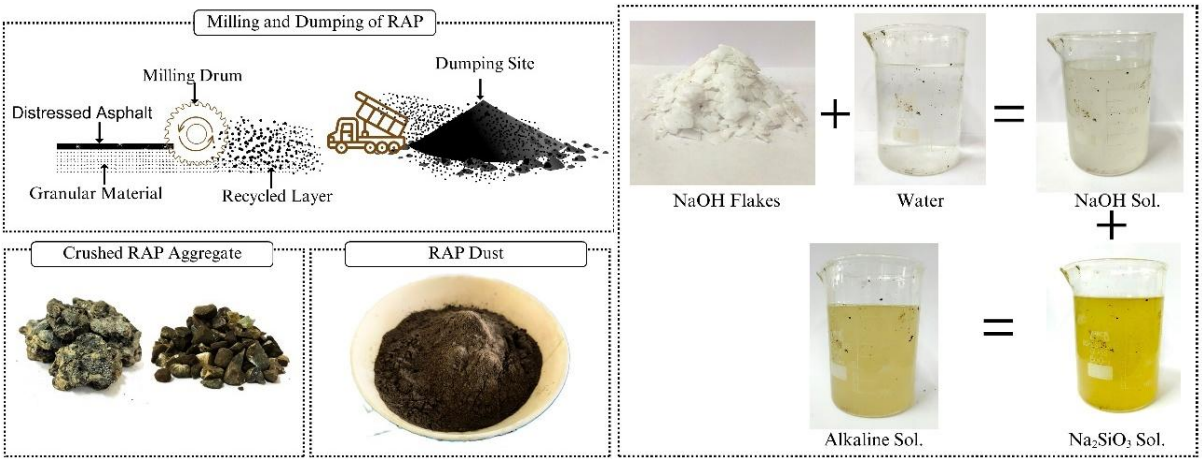

Figure 2. Material preparation for geopolymer mortar

The alkaline activators, sodium silicate solution (Na_2SiO_3), and sodium hydrate flakes (NaOH) were acquired from a local supplier (Garg Chemicals, Jalandhar, India). A detailed summary of the properties of the alkaline activator is presented in Table 1. The fine aggregates were sourced from a local distributor and subjected to washing and sun drying before use in geopolymer mortar. The physical properties of the fine aggregates, including the specific

gravity, fineness modulus, and water absorption, were determined to be 2,47; 2,54; and 1,62 %, respectively.

Table 1. Physical and chemical properties of the material used

Property	Material Type				
	RAP Dust	BA	FA	NaOH	Na_2SiO_3
Specific gravity	2,34	1,29	2,47	--	--
Fineness modulus	--	--	2,54	--	--
Water absorption (%)	--	--	1,62	--	--
Colour	Brown	Black	Brown	White	Off White
pH	--	--	--	13-14	13-14
Density (g/cm^3)	2,34	1,29	2,47	2,14	1,55
SiO_2	49,53	52,14	--	--	--
Al_2O_3	15,64	35,23	--	--	--
Fe_2O_3	14,32	1,67	--	--	--
CaO	11,28	19,47	--	--	--
MgO	0,58	1,73	--	--	--
SO_3	0,18	0,93	--	--	--
K_2O	1,47	0,87	--	--	--
Na (%)	--	--	--	58	9
O (%)	--	--	--	40	27
H (%)	--	--	--	2	64

2.2 Method

2.2.1 Mix and sample preparation

Table 2 shows the varying material proportions and ratios employed in the preparation of the 12 different mix design samples. These formulations encompassed varying percentages of RAP dust, including 0; 35; 65; and 100 %, as a substitute for BA. Additionally, the Na_2SiO_3/NaOH ratio was selected based on the results of previous studies conducted by different researchers to optimise the dissolution and polymerisation kinetics of aluminosilicate precursors, and thereby ensure adequate mechanical performance [29; 31; 34; 35; 45; 46]. A higher silicate content enhances geopolymerisation but may increase viscosity, which affects the ease of handling and working with the mortar. Three distinct ratios of Na_2SiO_3/NaOH (i.e 1,0R; 1,5R; and 2,0R) were selected to assess the influence of varying the alkalinity on the reaction kinetics and structural integrity of RAP dust and BA-based geopolymer mortars. Sodium hydrate flakes were meticulously mixed with water one day before geopolymer mortar production to ensure a consistent 10 M solution. First, the binder and sand were blended manually for 30 s. Then, the alkaline activator solution was carefully incorporated into the dry materials, and a second 60 s mixing cycle was used to create a new geopolymer (GP) mortar. The freshly prepared GP mortar was then poured into moulds and compacted on a vibrating table for 10 s, as shown in Figure 3. Subsequently, the GP mortar moulds underwent a 24 h curing period at ambient temperature and humidity (27 °C and 65 % relative humidity (RH)), covered with plastic sheets [47]. Subsequently, the specimens are transferred to a heated oven for an additional 48 h duration at 65 °C. This elevated temperature curing regime accelerated hydrolysis, polymerisation, and moisture removal, culminating in the formation of a more resilient and chemically bonded geopolymer material. Post-curing, the GP specimens were extracted from the moulds and stored under ambient temperature and humidity conditions (27 °C, 65 % RH) until subjected to testing at 3, 7, and 28 days [48; 49]. The geopolymer samples were denoted as 1R0, 1R35, 1R65, and 1R100, where the first digit depends on the

Na_2SiO_3/NaOH ratio and the last digit represents the percentage replacement of BA with RAP dust.

A comprehensive cost analysis was conducted to compare the economic feasibility of the developed geopolymer mortar with those of other geopolymer mortar formulations reported in the literature. The cost estimations were based on local material rates to ensure contextual relevance to the geographical location of the study. The analysis revealed that the proposed mix design exhibited a 14,12 % or greater reduction in the cost per cubic metre compared with conventional geopolymer mortar formulations. This cost efficiency is primarily attributable to the free availability of RAP dust and BA, which were sourced locally to significantly reduce binder material expenses. The incorporation of these industrial by-products not only enhances sustainability but also demonstrates the potential for large-scale economic viability in geopolymer mortar production.

Table 2. Mix design of geopolymer mortar (kg/m^3)

Mix	RAP Dust	Bagasse ash	Alkaline Solution/ Binder	Aggregate/ Binder	Na_2SiO_3/ NaOH	NaOH Sol
1,0R0	0	500	0,6268	3	1,00	156,7
1,0R35	175	325	0,6268	3	1,00	156,7
1,0R65	325	175	0,6268	3	1,00	156,7
1,0R100	500	0	0,6268	3	1,00	156,7
1,5R0	0	500	0,5224	3	1,50	104,5
1,5R35	175	325	0,5224	3	1,50	104,5
1,5R65	325	175	0,5224	3	1,50	104,5
1,5R100	500	0	0,5224	3	1,50	104,5
2,0R0	0	500	0,4700	3	2,00	78,3
2,0R35	175	325	0,4700	3	2,00	78,3
2,0R65	325	175	0,4700	3	2,00	78,3
2,0R100	500	0	0,4700	3	2,00	78,3

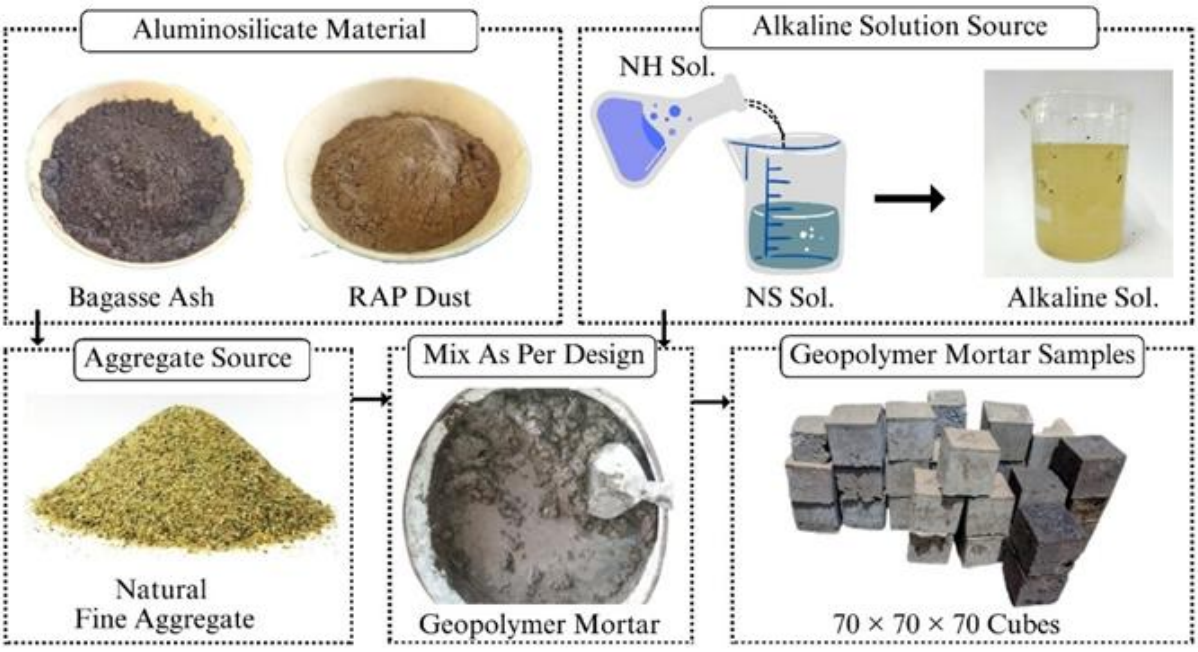

Figure 3. Sample preparation for geopolymer mortar

2.2.2 Compressive strength test

The compressive strength of geopolymer mortar was determined according to IS 1489 (Part 1) [50]. Three cubes of each mix design with a mould size of 70 × 70 × 70 mm were cast to check the compressive strength at 3, 7, and 28 days of age. The compression test was conducted using a compression testing machine (CTM) with the displacement control set at a rate of 5 mm/min, as shown in Figure 4. The compressive strength was calculated as follows: F_c=Pu/A, where Fc is the compressive strength in MPa, Pu is the applied ultimate load in N, and A is the loaded area in mm^2.

Figure 4. Compressive strength testing of geopolymer mortar specimens

2.2.3 Thermogravimetric analysis

The thermogravimetric analysis (TGA) procedure was conducted on the geopolymer matrix after 28 days of curing. The protocol involved a gradual temperature increase from 40-105 °C at a rate of 2 °C/min to eliminate extra water content from the samples. Subsequently, the temperature was maintained at 105 °C for 2 min to stabilise the mass loss before further escalating the temperature from 105-1000 °C at a rate of 10 °C/min to investigate the mass loss at various temperature intervals [2].

2.2.4 Scanning electron microscope

The microstructural properties of the mortars were meticulously examined using a SIGMA 500VP Field Emission Scanning Electron Microscope (SEM) operating at an accelerating voltage of 6-12 kV. Employing low-vacuum SEM, a comprehensive analysis of the microstructure was conducted across the sample width, which is particularly advantageous for delicate specimens, such as mortar, thus preventing the further damage that is often associated with conventional SEM techniques. In addition to the targeted investigations of specific regions of interest, the advanced single-point focusing capability of the SIGMA 500VP SEM enabled the partitioning of the entire sample area into discrete segments, with each segment meticulously magnified and seamlessly integrated, as shown in Figure 5. This technological process not only facilitates rapid spot inspections but also allows for the precise detection of microstructural variations along the length of an object, ensuring thorough data acquisition for future reference and analysis.

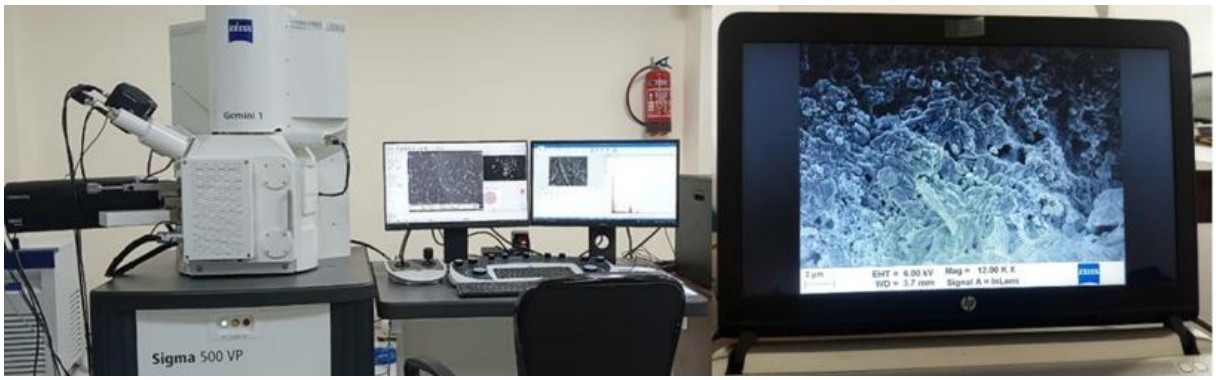

Figure 5. SEM testing of a geopolymer mortar specimen

2.2.5 X-ray diffraction

An X-ray diffraction (XRD) analysis was employed to assess the phase transformations occurring in BA-RAP dust-based geopolymer mortars at 28 days. Spectra were acquired for powdered samples extracted from both the degraded and intact cores. A cutting-edge PANalytical Empyrean XRD system was equipped with a 4 kW X-ray generator (capable of a maximum values of 60 kV and 100 mA). This system features an easy and tool-free point-focus switch for swift adjustments. The goniometer allows for a maximum usable range of -111° < 2θ < 168°, with a smallest addressable increment of 0,0001° and an angular reproducibility of less than 0,0002°, as shown in Figure 6.

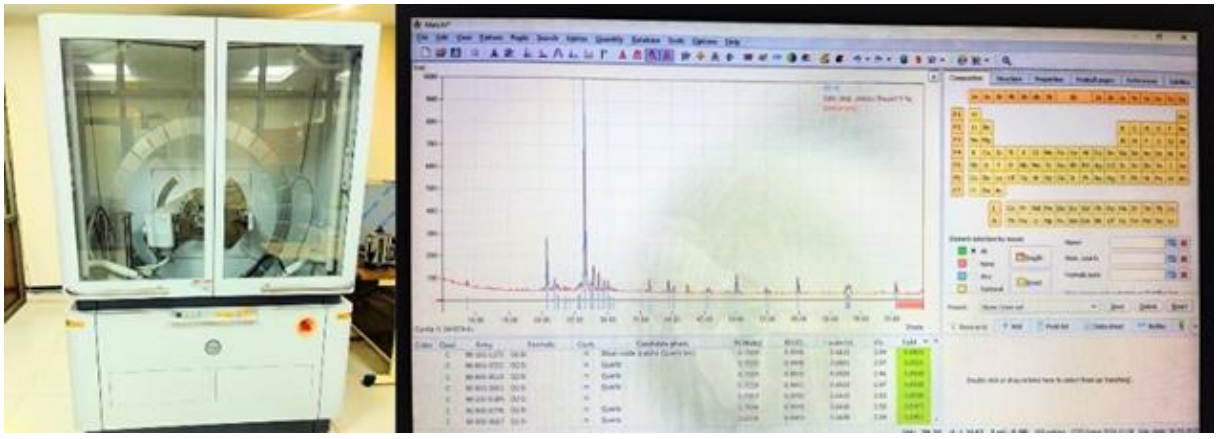

Figure 6. XRD testing of geopolymer mortar specimen

2.2.6 Fourier transform infrared spectroscopy

Chemical compounds present in geopolymer mortars, specifically, their chemical bond vibration spectra, were investigated via Fourier transform infrared (FTIR) spectroscopy. The FTIR analysis was conducted using a Bruker Alpha FTIR spectrometer. Spectra were collected over a range of 500 to 4000 cm^{-1}, with band identification referencing established patterns within the realm of silicate studies, as shown in Figure 7. The preparation of the sample pellet involved utilising a geopolymeric mortar sample that had been aged for 28 days, dried, and crushed finely to a particle size finer than 75 µm. Approximately 2-3 g of the sample was inserted into the infrared equipment with software activation using the specified parameters.

Figure 7. FTIR testing of a geopolymer mortar specimen

2.3 Statistical analysis

This study employed a diverse array of machine learning techniques to predict the compressive strengths of geopolymer mortars, meticulously selecting suitable methodologies for machine learning (ML) algorithms. The research context pertains to a practical machine learning problem called regression. Thus, regression algorithms, including the random forest regressor (RFR), gradient boost regressor (GBR), and extreme gradient boost regressor (XGBR) were used. The parameter settings for each machine learning model employed to investigate the geopolymer dataset were optimised to ensure optimal predictive performance.

2.3.1 Data collection

The novel dataset employed in this investigation comprises 331 observations generated via extensive existing studies. Each observation is characterised by three variables: the silicate-to-hydrate ratio, alkaline solution-to-binder ratio, and curing age (in days) sourced from prior studies [2; 11; 29-32; 47; 51-55]. In addition, quantitative measurements of compressive strength (in MPa) were incorporated into the dataset. The dataset was normalised to a range between zero and one using Eq. 1 to ensure uniform feature scaling and prevent variables with larger magnitudes from disproportionately influencing the analysis. To better capture the synergistic effects between the variables, interaction terms between the variables were introduced, which significantly improved the R^2 value of the model by explicitly encoding time-dependent chemical reaction dynamics. This normalisation facilitates a more balanced and accurate regression model. The primary objective was to analyse the interdependencies among the input variables and accurately predict the compressive strength of the mortar. Through regression analysis, this study aims to capture the complex nonlinear relationships governing the mortar strength and enhance the reliability of predictive modelling.

$$Z_{ij} = \frac{\max(V_i) - V_i}{\max(V_i) - \min(V_i)} \quad (1)$$

Where Z_{ij} represents normalised values, and V_i is a variable.

2.3.2 Model selection and evaluation

The GBR and XGBR stand as sophisticated ensemble learning methodologies within the realm of predictive modelling, akin to the esteemed RFR pioneered by L. Breiman [56]. Rooted in the foundation of decision trees, particularly the classification and regression tree (CART), these techniques intricately refine weak learners via iteration to bolster predictive accuracy [57]. GBR and XGBR operate based on the principle of sequentially constructing decision trees to rectify the errors introduced by preceding models. Whereas GBR amalgamates multiple decision trees, XGBR leverages a more advanced boosting algorithm, instead optimising model performance through meticulous gradient descent procedures [58]. In alignment with the RFR methodology, each constituent decision tree in GBR and XGBR functions autonomously and contributes independently to the ensemble output. This collective output is computed as the weighted aggregation of all individual tree predictions, which epitomises the essence of ensemble learning principles. Similar to RFR, both GBR and XGBR harness random subsets of observations and candidate variables for each tree. This strategy aims to fortify error estimation robustness and assuage potential data loss ramifications [57-59]. Paramount parameters governing the efficacy of these algorithms include the learning rate, tree depth, and regularisation, and each is meticulously fine-tuned to optimise the predictive performance and model generalisation across diverse datasets, as shown in Figure 8. The model parameters were rigorously optimised using state-of-the-art techniques. For RFR model particle swarm optimisation (PSO) with 50 iterations of an optimised tree count of 50-500, a sample size of 20-200, and a feature subset size of 2-8 were used. In contrast, for a GBR/XGBR grid search five-fold cross validation, a systematically evaluated depth of 3-6, learning rates of 0,01-0,10 and tree count of 100-200 were used.

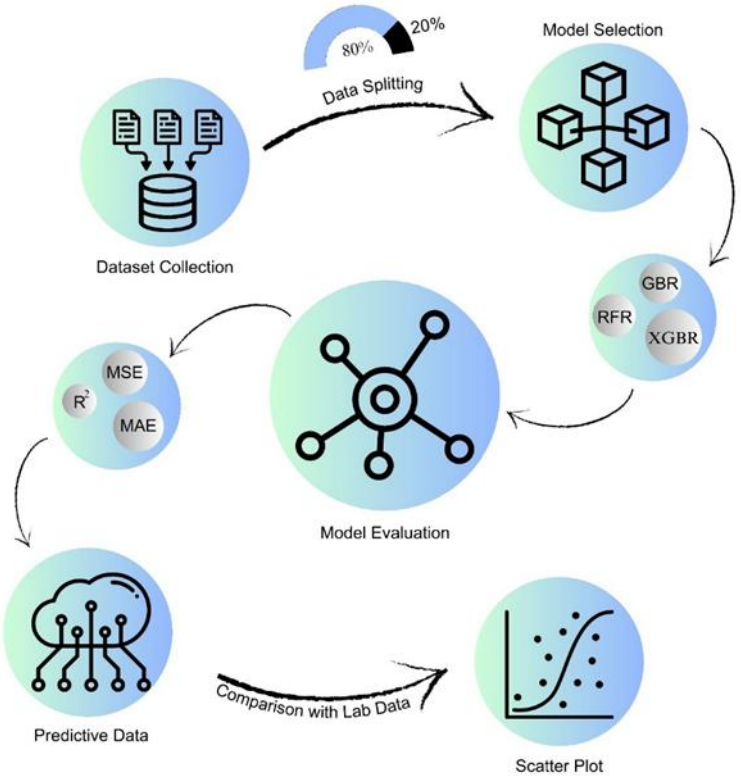

Figure 8. Framework for predicting the compressive strengths of geopolymer mortars

In regression analysis, R^2 serves as a crucial metric for assessing the goodness-of-fit of a model. The R^2 value quantifies the proportion of variance in the dependent variable (target) that can be attributed to the independent variables incorporated into the model. The R^2 values range between 0 and 1, with a higher value indicating more substantial explanatory power and a better fit of the model to the observed data [26]. The mean absolute error (MAE) is another essential metric used in model evaluation. The MAE measures the average absolute difference between the actual and predicted values. The MAE provides a straightforward measure of the model's accuracy, with lower MAE values signifying better predictive performance [27; 60]. One advantage of the MAE is its robustness to outliers because it considers the absolute difference without squaring the errors. The mean squared error (MSE) is a commonly utilised metric that quantifies the average squared difference between the actual and predicted values. The MSE penalises significant errors more than the MAE does, making the MSE more sensitive to outliers and emphasising the importance of minimising substantial errors. Lower MSE values indicate better model performance in terms of predictive accuracy and precision [26; 27; 60].

3 Results and discussion

3.1 Compressive strength

Compressive strength analyses are essential in evaluations of the performance and structural feasibility of geopolymer matrices incorporating RAP dust and BA. This study systematically assessed 12 distinct mix designs, each of which was tested using three cubic specimens in accordance with IS 1489 (Part 1) [50]. The primary variables investigated were the Na_2SiO_3/NaOH ratio and replacement levels of RAP dust (0; 35; 65; and 100 %) with BA, as detailed in Table 2. The experimental results revealed a progressive reduction in the compressive strength with increasing RAP dust replacement, which was attributable to the presence of asphalt residues that potentially hindered geopolymerisation. As illustrated in Figure 9, the compressive strength of the 1,0R series at 3 days of testing ranged from 0,15-2,5 MPa, following a similar trend at later ages, reaching values between 1,03 and 10,74 MPa at 7 days and 3,05-15,41 MPa at 28 days. This observed reduction in strength using an Na_2SiO_3/NaOH ratio of 1, particularly at higher RAP replacement levels, suggests that asphalt-coated particles interfere with aluminosilicate gel formation and thereby weaken the overall matrix structure at lower silicate-to-hydrate ratios.

In contrast, the 1,5R series exhibited improved strength retention compared with the 1,0R series, with values ranging from 3,98-6,71 MPa at 3 days, increasing to 8,86-18,69 MPa at 7 days and reaching 14,55-21,56 MPa at 28 days. The compressive strength results indicated that the lowest recorded strength in the 1,5R series at 28 days closely aligned with the highest strength achieved in the 1,0R series at the same curing age. This trend underscores the significant influence of the Na_2SiO_3/NaOH ratio on the geopolymerisation process and the resultant mechanical properties. This improvement is attributable to the optimised Na_2SiO_3/NaOH ratio, which enhances silica dissolution and geopolymerisation. The highest compressive strength values were recorded in the 2,0R series, where the early-age strength at 3 days varied between 7,88-10,69 MPa. At 7 and 28 days, the strengths ranged from 15,90-22,78 MPa and 17,78-27,05 MPa, respectively. Notably, a 1,84 % increase in compressive strength was observed when RAP dust replacement was limited to 35 %, indicating a potential threshold at which the pozzolanic activity of BA may partially compensate for RAP-induced strength losses at Na_2SiO_3/NaOH ratio of 2. This increased silicate content in the 2,0R series likely enhanced the dissolution of aluminosilicate precursors and thereby facilitated a denser geopolymer network and improved the strength development. In contrast, the lower Na_2SiO_3/NaOH ratios in the 1,0R and 1,5R series may have limited the availability of soluble silica species, thereby restricting the polymerisation reaction and leading to reduced compressive strength. This observation highlights the necessity of optimising the activator composition to achieve a superior mechanical performance in RAP-incorporated geopolymer matrices.

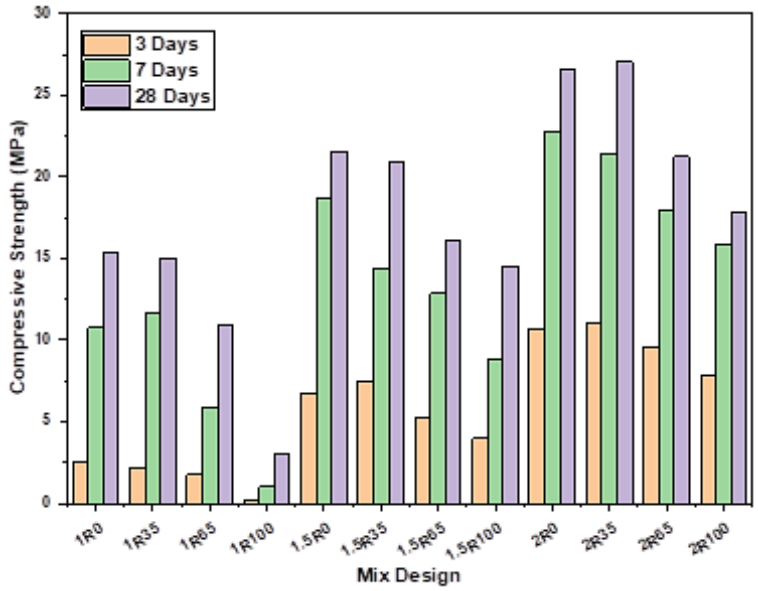

Figure 9. Compressive strength of geopolymer mortar

The graphical representation in Figure 9 further confirms the declining strength trend across all mix designs, emphasising the negative impact of RAP dust at higher replacement levels owing to its poor adhesion properties. These findings align with those of previous studies on RAP utilisation in cementitious systems. Rout, Roy, and Alwathaf also reported significant reductions in mechanical properties when RAP was introduced into concrete, primarily because of the residual asphalt film that weakens the bonding between particles [36; 61]. Similarly, Singh demonstrated that high RAP incorporation into a concrete matrix leads to compressive strength losses owing to disrupted reactions. In contrast, research on BA suggests that its high silica content enhances the long-term strength of ash-based geopolymers by promoting secondary pozzolanic reactions [62; 63]. The performance of RAP dust in the current study supports these findings and suggests that an optimal balance between RAP dust and BA can mitigate strength degradation and optimise geopolymerisation efficiency. From a practical perspective, the results underscore the necessity of optimising mix proportions to maintain structural integrity while promoting sustainable material utilisation. Testing suggests that RAP dust replacement levels should be restricted to 35 % or lower to prevent excessive strength reduction, particularly in applications requiring high compressive performance. The superior performance of the 2,0R series highlights the importance of adjusting the Na_2SiO_3/NaOH ratio to enhance the availability of soluble silica and improve geopolymerisation. Although a higher RAP content adversely affects the strength, moderate incorporation could still be viable for nonstructural applications in which lower compressive strength requirements are acceptable.

A machine learning approach was employed to compare and refine these finding using a diverse set of algorithms for compressive strength estimation. After hyperparameter optimisation and feature engineering, RFR emerged as the most accurate model, achieving an R^2 of 0,73; MSE of 583,76; and MAE of 23,56; as shown in Table 3. The GBR also demonstrated robust performance with an R^2 of 0,58 and MAE of 7,55 [64]. This deviation is attributable to the complex structure of the geopolymer matrix and lack of research data on novel RAP dust waste materials.

Conversely, the XGBR model exhibits comparatively poor performance, with an MSE of 504,57; MAE of 19,67; and R^2 of 0,57. These results highlight the substantial disparities of approximately 78.85% in MSE and 67,95 % in MAE between the RFR and GBR models. Moreover, the R^2 values differed by approximately 20%. These predicted compressive strength values are closely aligned with the actual compressive strength values and show promising

correlations, as shown in Figure 10. The optimised models enabled the practical prediction of the strength development in geopolymer mortar. For instance, simulating curing ages from 3 to 28 days with varying SS/SH ratios (1,0; 1,5; and 2,0), the RFR model predicts strength gains from 24,68-52,58 MPa. These predictions are critical for quality control in the construction industry. These models can be further leveraged to optimise the activator dosage in the target computational mixture design [2; 11; 29-32; 47; 51-55]. Using these models, trial batches can be reduced by 40-60 % through a computational mixture design. This approach can also predict long-term durability by extrapolating curing-age relationships. This data-driven approach reduces material waste and accelerates sustainable geopolymer adoption.

Table 3. Machine learning model predictions

Predictive Parameters	R^2	MAE	MSE
RFR	0,73	23,56	583,76
GBR	0,58	7,55	123,46
XGBR	0,57	19,67	504,57

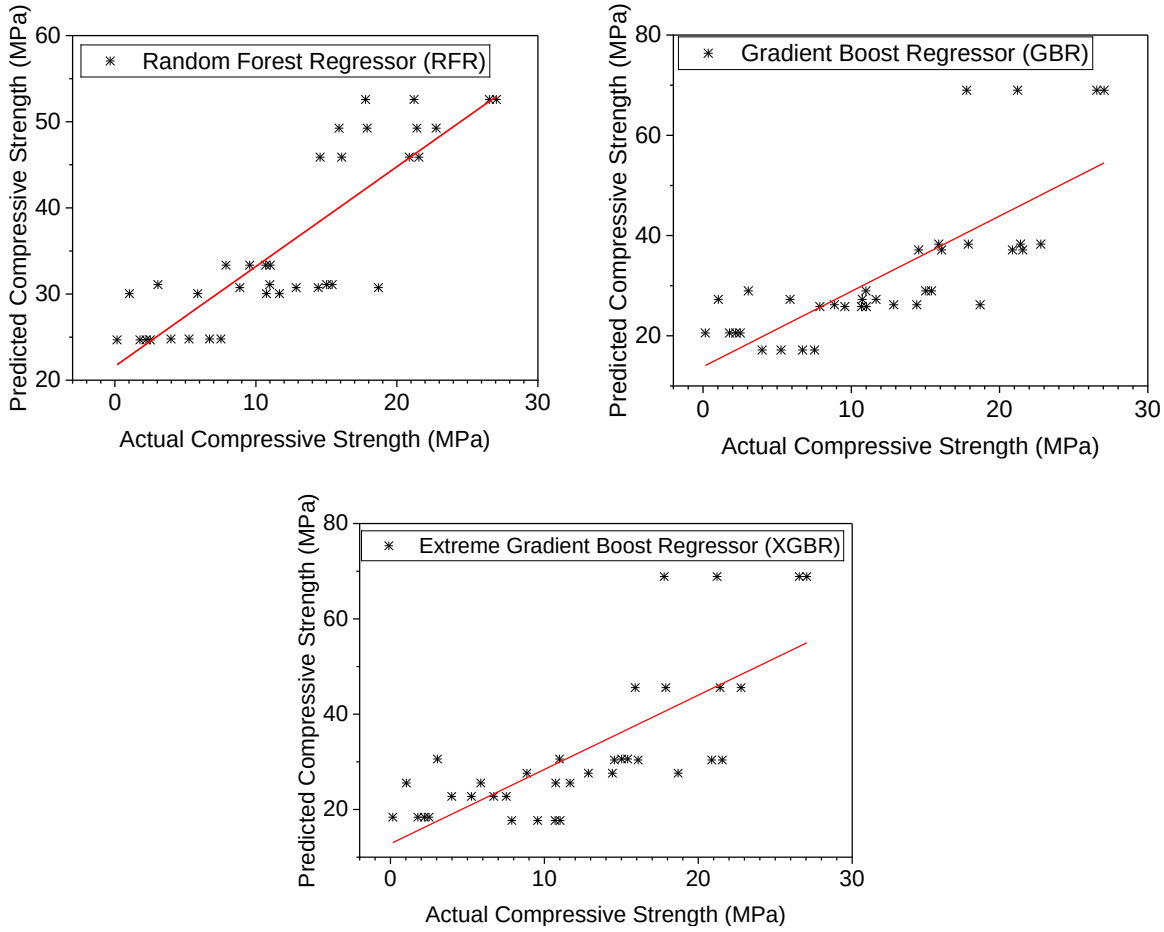

Figure 10. Comparison between predictive and actual compressive strengths (MPa)

3.2 Thermogravimetric analysis

The TGA curve shown in Figure 11 serves as a crucial tool for elucidating the changes in mass (g) as a function of increasing temperature, and it offers profound insights into the thermal behaviours of different geopolymer mortar mixes (1,0R0; 1,0R35; 1,0R65; 1,0R100; 1,5R0;

1,5R35; 1,5R65; 1,5R100; 2,0R0; 2,0R35; 2,0R65 and 2,0R100). The mass loss trend observed in the temperature range of ambient to 1000 °C highlights the decomposition of different phases within the geopolymer matrix [52]. In the initial stage (ambient to 105 °C), a significant weight loss occurs owing to the evaporation of free water, which is primarily absorbed within the porous structure of the geopolymer. This initial dehydration process is critical because it influences the early stage shrinkage and cracking potential of the material. The least variation in the initial stage was observed in the mixes with high amounts of RAP dust and low Na_2SiO_3/NaOH ratios. These results are primarily attributable to the lower availability of free water absorbed from the atmosphere within the matrix, which results in a reduced initial moisture loss. The presence of residual bitumen particles in RAP dust also imparts some degree of hydrophobicity, which limits moisture uptake and subsequently minimises early stage evaporation. Furthermore, the higher RAP dust content contributed to the formation of thermally stable phases, which enhanced the resistance of the material to initial weight loss by reducing the extent of dehydration and structural degradation at lower temperatures.

The second stage (105-400 °C) corresponds to the loss of structural water associated with NASH (Na-Al-Si-H) gel, which is a primary binding phase in geopolymers. The weight reduction trend suggests that mixes with lower Na_2SiO_3/NaOH ratios (such as the 1,0R series) exhibited a relatively higher mass loss within this temperature range, indicating a less compact gel structure and more significant degree of dehydration. For instance, the 1,0R0 mix exhibits a weight reduction of 22 g, whereas the 2,0R100 mix experiences a lower relative loss of 13 g over the same temperature range. This pattern also highlights that mixes with lower RAP dust contents and lower Na_2SiO_3/NaOH ratios tend to exhibit higher dehydration rates up to 400 °C. These outcomes likely resulted owing to the presence of a more porous and loosely bonded geopolymer network. Conversely, mixes with higher Na_2SiO_3/NaOH ratios, such as the 1.5R and 2R series, demonstrated slightly lower weight losses, suggesting improved polymerisation and a denser N-A-S-H gel structure. For example, the 2,0R0 mix showed a loss of 12 g, indicating a more gradual mass loss than those of the 1,0R0 and 1,5R0 mixes. These findings emphasise the role of mix composition in influencing thermal stability, with higher Na_2SiO_3/NaOH ratios contributing to improved resistance to early stage mass loss [2].

Between 400 and 600 °C, the geopolymer matrix exhibits relative thermal stability, with minimal mass loss observed across all mix series. However, structural reorganisation begins to occur within the material, which leads to matrix densification and a reduction in the overall porosity owing to the collapse of microvoids and partial sintering of the geopolymer network. Among the studied series, the 2,0R mixtures exhibited the lowest mass losses in this temperature range, indicating a more thermally stable microstructure and reduced dehydration of the bound phases. These results suggest that the RAP dust and BA binder, in combination with a higher Na_2SiO_3/NaOH ratio, contributed to a more resilient framework under this range of thermal exposure. In contrast, the 1,0R series experienced a relatively higher weight loss than did the other two series, suggesting a greater degree of dehydration of the other hydrous aluminate phases and structural water loss. However, despite this increased mass loss, the 1R series demonstrates improved thermal resistance in this range compared with its behaviour in the range of 105-400 °C, thus indicating a progressive stabilisation of the geopolymer matrix beyond initial dehydration. At higher temperatures (600-1000 °C), significant transformations occur, leading to a notable weight loss ranging from 5,87-6,77 % in the 1,0R series, 6,06-7,56 % in the 2,0R series, and 6,14-7,21 % in the 1,5R series. This mass reduction is attributable to the breakdown of the geopolymer network, dehydroxylation of the residual phases, and potential formation of crystalline phases [52; 65]. These changes correlate with strength deterioration at elevated temperatures, as shown in Figure 12.

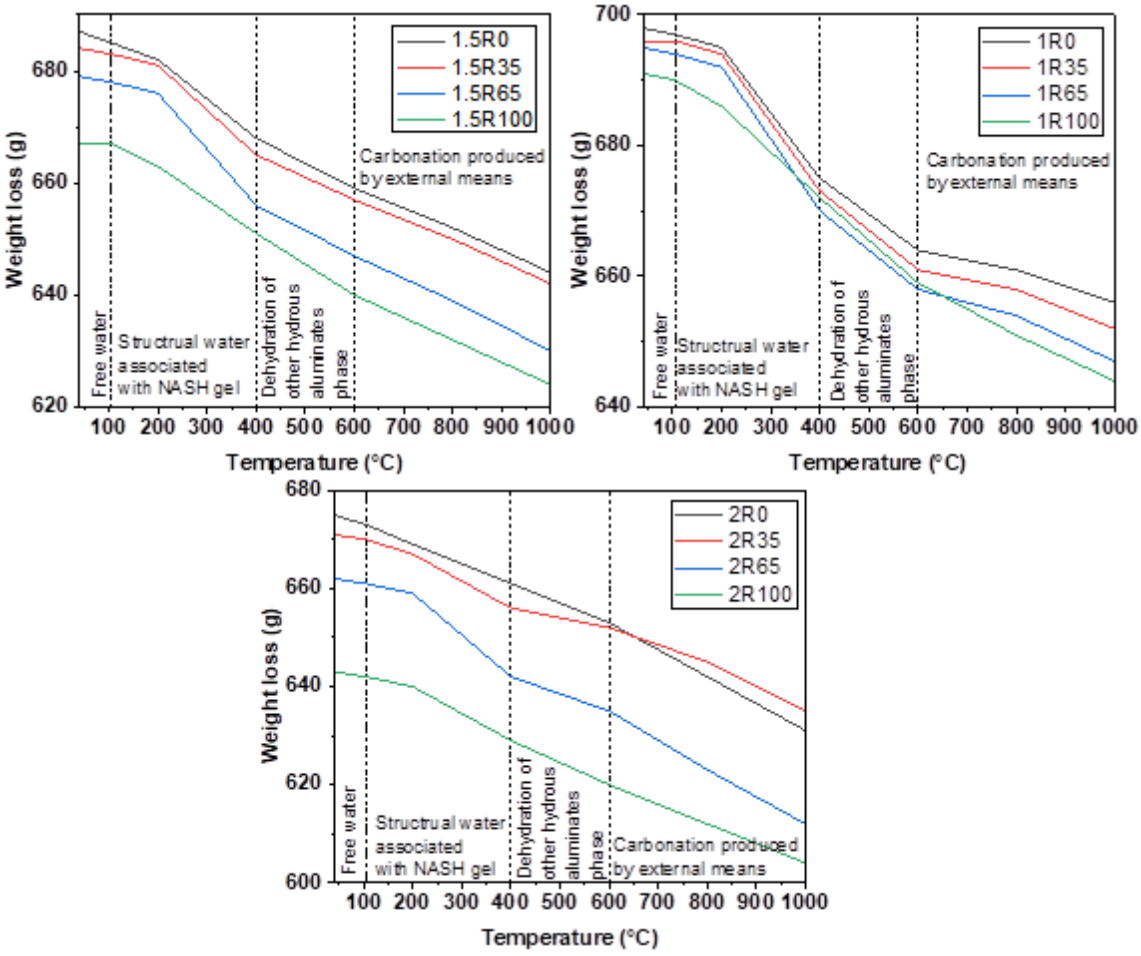

Figure 11. Thermogravimetric analysis of geopolymer mortars

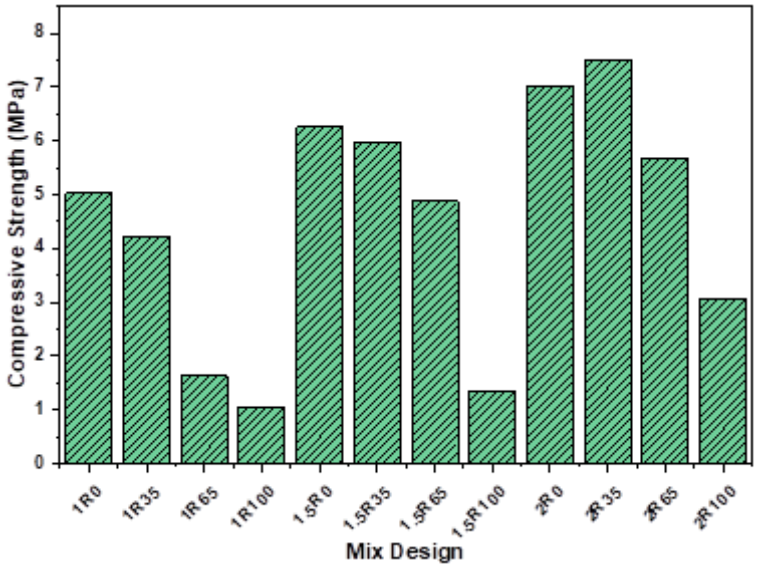

Figure 12. Compressive strengths after TGA analysis

The TGA analysis offers comprehensive insight into the thermal behaviour of various geopolymer mortar mixes that which are characterised by distinct effects on the compressive strength after exposure to 1000 °C, as shown in Figure 12, and density at an ambient

temperature, as shown in Figure 13. Analyses of the results revealed nuanced variations that were attributable to differences in mix composition and processing conditions, thereby elucidating the intricate interplay between the material constituents, Na2SiO3/NaOH ratio, and thermal degradation phenomena [55; 66]. Among the studied mix designs, the 2R series exhibits relatively higher compressive strengths compared with those of the 1,0R and 1,5R series after exposure to the highest temperature of 1000 °C. Mixes labelled 1,0R0; 1,0R35; 1,0R65; and 1,0R100 demonstrate compressive strengths ranging from 1,05-5,02 MPa, reflecting the influence of mix parameters, such as the ratio of Na_2SiO_3/NaOH and replacement ratio of RAP dust with BA as a precursor, with higher ratios resulting in reduced strength. Similarly, the 2,0R series, characterised by higher RAP dust values, exhibits lower compressive strengths, with 2,0R0; 2,0R35; 2,0R65; and 2,0R100 recording strengths ranging from 3,06-7,02 MPa.

This trend suggests a trade-off between the strength, Na_2SiO_3/NaOH ratio, and replacement ratio of the precursor, highlighting the importance of optimising the mix proportions to achieve the desired performance characteristics. Furthermore, the density values of the geopolymer mortar mixes exhibited a similar trend, with higher Na_2SiO_3/NaOH ratios and higher RAP dust replacement values correlating with lower densities across all mix designs. Mixes with lower R values (1,0R series) generally demonstrate higher densities, which are attributable to the efficient packing and excellent compaction of materials or the higher water content in the mix. For instance, 1,0R0; 1,0R35; 1,0R65; and 1,0R100 exhibit density ranging from 1960,48-1981,02 kg/m^3 at an ambient temperature, which is indicative of their denser microstructures or greater water contents compared with the 2,0R series, where the density ranges from 1825.24 to 1914,84 kg/m^3.

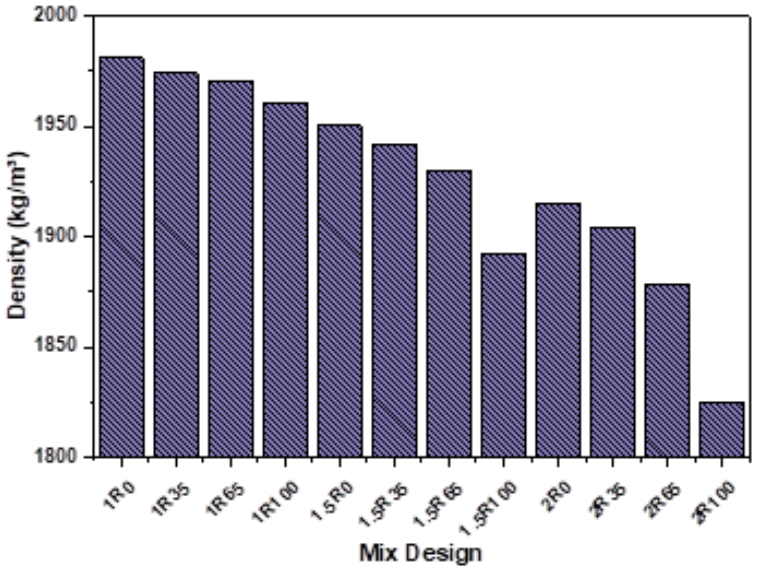

Figure 13. Densities of geopolymer mortars

The observed variations in the compressive strength, density, and weight at various temperatures among the different mix designs are attributable to factors such as the type and proportion of raw materials, curing regime, and Na_2SiO_3/NaOH concentration. Adjusting these parameters allows for the customisation of geopolymer mortar properties to suit specific application requirements, such as structural integrity, thermal stability, and density optimisation. Overall, a comprehensive analysis of TGA data in conjunction with compressive strength and density measurements provides valuable insights into the thermal behaviour and mechanical performance of geopolymer mortar mixes [55; 66; 67]. The intricate relationships between the mix composition, material properties, and Na_2SiO_3/NaOH ratio were elucidated. By integrating these techniques, this study effectively correlates the thermal stability, phase

composition, and integrity with the reduction in weight and mechanical properties, thus guiding the optimisation of geopolymer mortar formulations for high-temperature applications.

3.3 Scanning electron microscopy analysis

The SEM analysis provides an in-depth examination of the microstructure and morphology of geopolymer mortars, offering crucial insights into the composition and properties of critical phases, such as calcium silicate hydrate (C-S-H), calcium aluminium silicate hydrate (C-A-S-H), and sodium aluminium silicate hydrate (N-A-S-H). Through careful examinations of SEM images, the intricate microstructural features of geopolymer mortars can be analysed to gain a deeper understanding of their mechanical and thermal behaviours. In the case of the 2,0R35 geopolymer matrix, the SEM analysis yielded significant and revealed distinctive microstructural characteristics. Notably, the presence of a dense and interconnected C-S-H gel was evident, underscoring its pivotal role in enhancing the mechanical strength and thermal stability of the material [51].

The morphology of C-A-S-H phases, characterised by cloud-like structures, as shown in Figure 14, signifies the incorporation of aluminium into the geopolymer network, thereby influencing its chemical and mechanical properties [52]. Additionally, SEM imaging provides valuable insights into the formation and distribution of the N-A-S-H gel, which is a critical component in the early stage hydration of geopolymers [29; 68]. The presence of dark spherical cloud-like structures and fibrous networks of the N-A-S-H gel within the geopolymer matrix highlights its significant contribution to the adhesive properties and overall microstructural integrity of the material. Comparing the SEM images of the specimens before and after exposure to high temperatures revealed a transition from a dense, well-packed structure at ambient temperature to a progressively more porous and fractured morphology as the temperature increased. At temperatures exceeding 600 °C, microcracks and voids become more prominent, indicating the onset of thermal degradation and the loss of binding phases [52]. This structural degradation aligns with the observed decrease in compressive strength, as shown in Figure 12. These SEM findings were further corroborated via the XRD analysis, which identified the presence of crystalline phases, such as quartz and albite, within the geopolymer matrix.

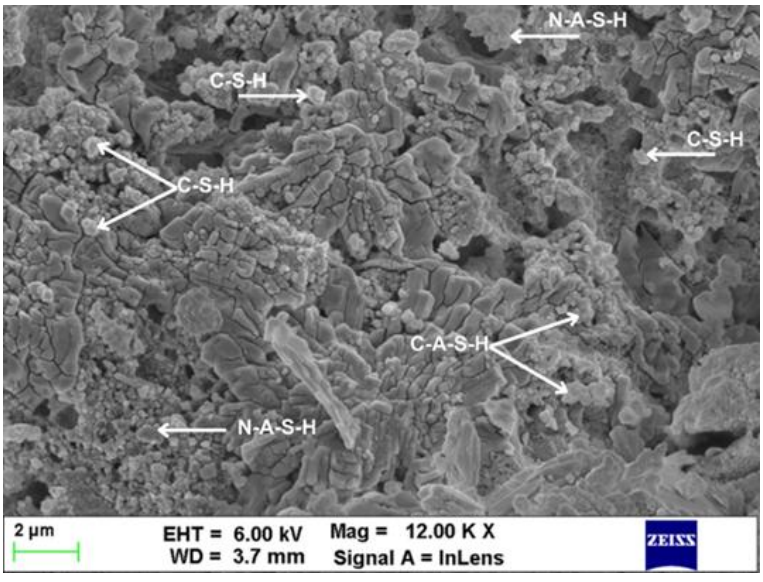

Figure 14. SEM analysis of geopolymer mortar (2,0R35) at 28 days

3.4 X-ray diffraction analysis

XRD analysis is a fundamental technique used in the microstructural study of geopolymer mortars, offering profound insights into their crystalline structures and phase compositions. The mineralogical makeup of the geopolymer mortar matrices 2,0R35; 2,0R65; and 2,0R100

were analysed with precision and depth. Quartz, which is a ubiquitous mineral within geopolymer matrices, exhibits distinct diffraction peaks in XRD spectra. These peaks are observable at characteristic 2θ angles, such as 20,86°; 26,65°; 39,49°; and 42,47° as shown in Figure 15, signifying the presence of quartz crystals [52].

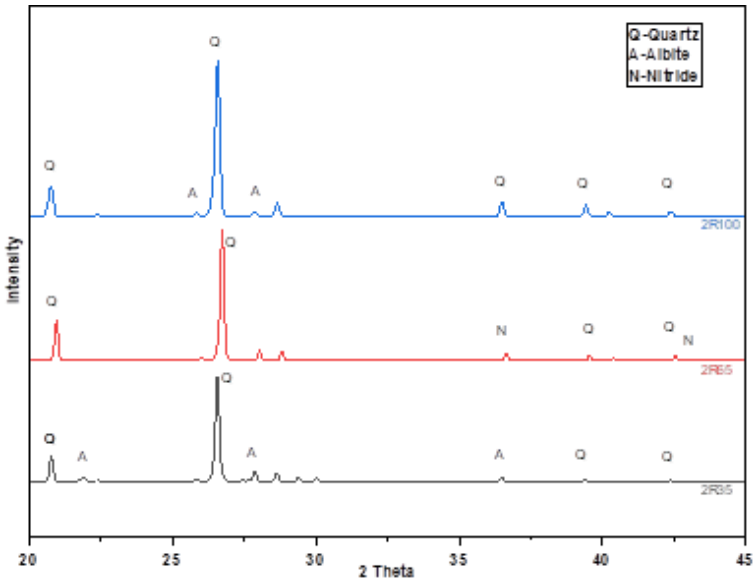

Figure 15. XRD analysis of geopolymer mortar

The intensities and positions of these peaks provide critical insights into the crystalline nature of quartz within the geopolymer matrix. XRD analysis enabled the identification of nitride phases at 36,65° and 42,55°; which may have originated from the presence of nitrogen or impurities in RAP dust. By examining the XRD patterns, the low or delayed strength of 2,0R65 can be discerned from the nitride phases, thereby unravelling their roles and influences on the composition and structural properties of the material. Additionally, XRD facilitated the detection of albite, which is a prevalent sodium aluminium silicate mineral found in geopolymer matrices, at 22,02°; 27,96° and 36,58°, correlating with the highest compressive strength and thermal stability achieved by the 2R35 geopolymer mortar sample [30]. The XRD analysis complements these findings by identifying the phase transitions occurring at different temperatures. During initial testing at an ambient temperature, the amorphous NASH gel dominated the structure. However, at higher temperatures (600-1000 °C), the formation of crystalline phases, such as nepheline and sodalite, is evident and leads to embrittlement and strength loss. The presence of unreacted precursors in high RAP dust is attributable to the low Na_2SiO_3 ratio, such as that in the 1,0R series. Incomplete geopolymerisation contributes to the overall lower thermal resistance and compressive strength after high-temperature exposure, as shown in Figures 11 and 12, respectively.

3.5 Fourier transform infrared spectroscopy

FTIR spectroscopy plays a vital role in the examination of geopolymer mortars and elucidation of their molecular structures and compositions. Through FTIR testing, the intricate chemistry and molecular structure of the different geopolymer formulations (2,0R0; 2,0R35; 2,0R65; and 2,0R100) were analysed. At a wavelength of around 943 cm^{-1}, a peak indicating Si-O stretching was observed. These results indicate that silicon-oxygen bonds form the backbone of the geopolymer network. These bonds are crucial for the strength and stability of the material and form aluminosilicate precursors under alkaline conditions. Additionally, a peak at approximately 1384 cm^{-1} suggested Al-O-Si stretching, indicating the presence of aluminium in the geopolymer mortar [65].

The detection of C-O stretching vibrations at approximately 1637 cm^{-1} indicates the presence of carbonates, which can be due to the use of BA/ RAP dust or atmospheric carbonation. Understanding the carbonate levels is essential for predicting material durability over time. Furthermore, the presence of Si-H stretching vibrations at approximately 2311 cm^{-1} suggests the existence of silicon-hydrogen bonds that likely originate from residual compounds. These bonds affect the adhesion properties and interactions of the material, thereby directly affecting the compressive strength of the geopolymer mortar. Finally, the peak corresponding to the O-H stretching vibrations at approximately 3587 cm^{-1} indicates the presence of water molecules, which are crucial for the geopolymer hydration process and overall structure [2]. Hence, the FTIR analysis provided valuable insights into the molecular makeup of geopolymer mortars, and thereby guided the development of tailored formulations for various construction requirements, as shown in Figure 16.

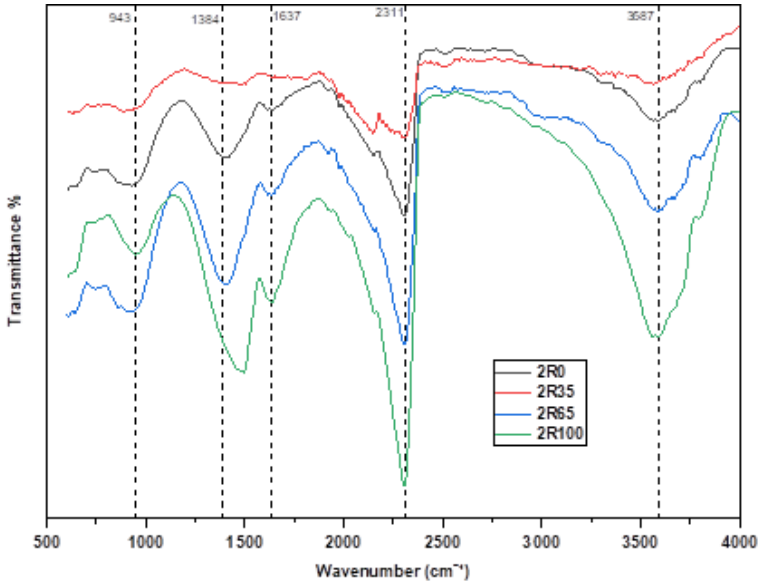

Figure 16. FTIR analysis of different geopolymer mortars

4 Conclusion

This research discusses the study of geopolymer mortars with varying ratios of novel waste materials, such as RAP dust and bagasse ash as a precursor. Different Na_2SiO_3/NaOH ratios and the impacts of their variations are also analysed and depicted in this study.

A compressive strength analysis revealed a nuanced relationship between the mix composition and mechanical properties. Variations in the Na_2SiO_3/NaOH ratio and RAP dust replacement percentage had significant effects on the compressive strength at 3, 7, and 28 days. Notably, although the compressive strength exhibited a declining trend with increasing RAP dust replacement, a marginal increase of 1.84% was observed in the 2R series with 35% RAP dust replacement. The decline in strength was primarily attributable to variations in the Na_2SiO_3/NaOH ratio and an increase RAP dust replacement.

- A dataset comprising 331 experimental observations was generated from extensive studies. Among the evaluated machine learning models, RFR outperformed GBR and XGBR, achieving an R^2 value of 0,73; MAE of 23,56; and MSE of 583,76; thus demonstrating its effectiveness in predicting geopolymer mortar performance.
- A TGA analysis offered crucial insights into the thermal behaviour of geopolymer mortars up to 1000 °C, revealing mass loss phenomena of 6,06-7,56 % in geopolymer mortars of series 2,0R. Mass losses of 6,14-7,21 % are observable along with declining compressive strength in the 1,5R series owing to the disintegration of the integrity of the geopolymer matrix.

- Microstructural analyses provided invaluable insights into the microstructural, crystalline, and molecular characteristics of geopolymer mortars. SEM was used to identify the formation of C-S-H, N-A-S-H, and C-A-S-H, and the results showed a prolonged gain of strength. High quartz peak and low albite peaks were observed in XRD, showing mineral stability. Moreover, an FTIR analysis revealed Si-O, Al-O-Si and C-O stretching at different wavelengths.

In conclusion, this study provides practical insights for optimising geopolymer mortar mix designs. A Na_2SiO_3/NaOH ratio of 2 with 35 % RAP dust replacement in the 2,0R series is recommended to achieve balanced strength and sustainability in construction applications. Field-scale implementation should assess the workability, durability, and structural performance under real-world conditions. Future research should focus on long-term durability, field trials, and curing optimisation to enhance the performance while minimising energy use. Life-cycle assessment and machine learning integration can further refine sustainability and predictive accuracy. By utilising industrial byproducts, this approach mitigates landfill waste, reduces the reliance on traditional binders, and lowers the carbon footprint, thereby advancing the development of sustainable construction materials. Addressing these gaps will advance the development of cost-effective high-performance geopolymer materials for diverse engineering applications.

Abbreviations

BA	Bagasse Ash
C-A-S-H	Calcium Aluminum Silicate Hydrate
CO_2	Carbon Dioxide
C-S-H	Calcium Silicate Hydrate
FTIR	Fourier Transform Infrared Spectroscopy
GBR	Gradient Boosting Regression
ML	Machine Learning
MSE	Mean Squared Error
N-A-S-H	Sodium Aluminum Silicate Hydrate
Na_2SiO_3	Sodium Silicate
NaOH	Sodium Hydroxide
RAP	Recycled Asphalt Pavement
R^2	Coefficient of Determination (R-squared)
RFR	Random Forest Regression
SEM	Scanning Electron Microscopy
TGA	Thermogravimetric Analysis
XGBR	Extreme Gradient Boosting Regression
XRD	X-ray Diffraction

References

[1] Davidovits, J. Geopolymers. *Journal of thermal analysis*, 1991, 37 (8), pp. 1633-1656. https://doi.org/10.1007/BF01912193

[2] Alloul, A.; Amar, M.; Benzerzour, M.; Abriak, N.-E. A comparative analysis of ambient-cured metakaolin geopolymer mortar and flash-calcined soil geopolymer. *Construction and Building Materials*, 2023, 409, 134085. https://doi.org/10.1016/j.conbuildmat.2023.134085

[3] Alrefaei, Y.; Dai, J.-G. Tensile behavior and microstructure of hybrid fiber ambient cured one-part engineered geopolymer composites. *Construction and Building Materials*, 2018, 184, pp. 419-431. https://doi.org/10.1016/j.conbuildmat.2018.07.012

[4] Habert, G.; d'Espinose de Lacaillerie, J. B.; Roussel, N. An environmental evaluation of geopolymer based concrete production: reviewing current research trends. *Journal*

of Cleaner Production, 2011, 19 (11), pp. 1229-1238. https://doi.org/10.1016/j.jclepro.2011.03.012

[5] Kuang, F. et al. Experimental study on high temperatures performance of rubberized geopolymer mortar. *Journal of Building Engineering*, 2023, 76, 107091. https://doi.org/10.1016/j.jobe.2023.107091

[6] Nazari, A.; Bagheri, A.; Riahi, S. Properties of geopolymer with seeded fly ash and rice husk bark ash. *Materials Science and Engineering: A*, 2011, 528 (24), pp. 7395-7401. https://doi.org/10.1016/j.msea.2011.06.027

[7] Okoye, F. N.; Durgaprasad, J.; Singh, N. B. Fly ash/Kaolin based geopolymer green concretes and their mechanical properties. *Data in Brief*, 2015, 5, pp. 739-744. https://doi.org/10.1016/j.dib.2015.10.029

[8] Hardjito, D. et al. On the Development of Fly Ash-Based Geopolymer Concrete. *Materials Journal*, 2004, 101 (6), pp. 467-472. https://doi.org/10.14359/13485

[9] Duxson, P.; Provis, J. L.; Lukey, G. C.; van Deventer, J. S. J. The role of inorganic polymer technology in the development of 'green concrete'. *Cement and Concrete Research*, 2007, 37 (12), pp. 1590-1597. https://doi.org/10.1016/j.cemconres.2007.08.018

[10] Sarker, P. K.; Kelly, S.; Yao, Z. Effect of fire exposure on cracking, spalling and residual strength of fly ash geopolymer concrete. *Materials & Design*, 2014, 63, pp. 584-592. https://doi.org/10.1016/j.matdes.2014.06.059

[11] Kul, A. et al. Characterization and life cycle assessment of geopolymer mortars with masonry units and recycled concrete aggregates assorted from construction and demolition waste. *Journal of Building Engineering*, 2023, 78, 107546. https://doi.org/10.1016/j.jobe.2023.107546

[12] Asteris, P. G.; Kolovos, K. G. Self-compacting concrete strength prediction using surrogate models. *Neural Computing and Applications*, 2019, 31 (Suppl1), pp. 409-424. https://doi.org/10.1007/s00521-017-3007-7

[13] Gupta, P.; Gupta, N.; Saxena, K. K.; Goyal, S. A novel hybrid soft computing model using stacking with ensemble method for estimation of compressive strength of geopolymer composite. *Advances in Materials and Processing Technologies*, 2022, 8 (sup3), pp. 1494-1509. https://doi.org/10.1080/2374068X.2021.1945271

[14] Ramagiri, K. K.; Boindala, S. P.; Zaid, M.; Kar, A. Random Forest-Based Algorithms for Prediction of Compressive Strength of Ambient-Cured AAB Concrete—A Comparison Study. In: *Proceedings of SECON'21 - Structural Engineering and Construction Management*, Marano, G. C. et al. (eds.). May 12-15, 2021, Springer; 2022, pp. 717-725. https://doi.org/10.1007/978-3-030-80312-4_61

[15] Li, Y. et al. The data-driven research on bond strength between fly ash-based geopolymer concrete and reinforcing bars. *Construction and Building Materials*, 2022, 357, 129384. https://doi.org/10.1016/j.conbuildmat.2022.129384

[16] Wang, Q. et al. Application of Soft Computing Techniques to Predict the Strength of Geopolymer Composites. *Polymers*, 2022, 14 (6), 1074. https://doi.org/10.3390/polym14061074

[17] Dai, Y. et al. A novel machine learning model to predict the moment capacity of cold-formed steel channel beams with edge-stiffened and un-stiffened web holes. *Journal of Building Engineering*, 2022, 53, 104592. https://doi.org/10.1016/j.jobe.2022.104592

[18] Fang, Z. et al. A novel machine learning method to investigate the web crippling behaviour of perforated roll-formed aluminium alloy unlipped channels under interior-two flange loading. *Journal of Building Engineering*, 2022, 51, 104261. https://doi.org/10.1016/j.jobe.2022.104261

[19] Paruthi, S. et al. A review on material mix proportion and strength influence parameters of geopolymer concrete: Application of ANN model for GPC strength prediction. *Construction and Building Materials*, 2022, 356, 129253. https://doi.org/10.1016/j.conbuildmat.2022.129253

[20] Ardhira, P. J.; Sathyan, D. A comparative study of normal and self-compacting geopolymer mortar and its strength prediction using tensor flow approach. *Materials Today: Proceedings*, 2022, 65 (Part 2), pp. 1046-1055. https://doi.org/10.1016/j.matpr.2022.04.139

[21] Shah, S. F. A.; Chen, B.; Zahid, M.; Ahmad, M. R. Compressive strength prediction of one-part alkali activated material enabled by interpretable machine learning. *Construction and Building Materials*, 2022, 360, 129534. https://doi.org/10.1016/j.conbuildmat.2022.129534

[22] Ahmad, A.; Ahmad, W.; Aslam, F.; Joyklad, P. Compressive strength prediction of fly ash-based geopolymer concrete via advanced machine learning techniques. *Case Studies in Construction Materials*, 2022, 16, e00840. https://doi.org/10.1016/j.cscm.2021.e00840

[23] Zhang, B.; Yan, B.; Li, Y. Study on mechanical properties, freeze–thaw and chlorides penetration resistance of alkali activated granulated blast furnace slag-coal gangue concrete and its mechanism. *Construction and Building Materials*, 2023, 366, 130218. https://doi.org/10.1016/j.conbuildmat.2022.130218

[24] Kanagaraj, B. et al. Investigation of physical, chemical, mechanical, and microstructural properties of cement-less concrete – state-of-the-art review. *Construction and Building Materials*, 2023, 365, 130020. https://doi.org/10.1016/j.conbuildmat.2022.130020

[25] Alexander, A. E.; Shashikala, A. P. Studies on the microstructure and durability characteristics of ambient cured FA-GGBS based geopolymer mortar. *Construction and Building Materials*, 2022, 347, 128538. https://doi.org/10.1016/j.conbuildmat.2022.128538

[26] Huo, W. et al. Development of machine learning models for the prediction of the compressive strength of calcium-based geopolymers. *Journal of Cleaner Production*, 2022, 380 (part 2), 135159. https://doi.org/10.1016/j.jclepro.2022.135159

[27] Kioumarsi, M.; Dabiri, H.; Kandiri, A.; Farhangi, V. Compressive strength of concrete containing furnace blast slag; optimized machine learning-based models. *Cleaner Engineering and Technology*, 2023, 13, 100604. https://doi.org/10.1016/j.clet.2023.100604

[28] Liu, M. et al. Effect of ground concrete waste as green binder on the micro-macro properties of eco-friendly metakaolin-based geopolymer mortar. *Journal of Building Engineering*, 2023, 68, 106191. https://doi.org/10.1016/j.jobe.2023.106191

[29] Zheng, C. et al. Development of a novel rapid repairing agent for concrete based on GFRP waste powder/GGBS geopolymer mortars. *Journal of Building Engineering*, 2023, 71, 106542. https://doi.org/10.1016/j.jobe.2023.106542

[30] Jiao, Z. et al. Chloride resistance of class C/class F fly ash-based geopolymer mortars with different strength grades. *Case Studies in Construction Materials*, 2023, 18, e01811. https://doi.org/10.1016/j.cscm.2022.e01811

[31] Thakkar, S.; Chanda, A.; Rawat, S. Early strength development of self-compacting geopolymer mortar using binary and tertiary blends of industrial wastes. *Materials Today: Proceedings*, 2023, 93 (Part 3), pp. 467-474. https://doi.org/10.1016/j.matpr.2023.08.089

[32] Bezabih, T.; Kanali, C.; Thuo, J. Effects of teff straw ash on the mechanical and microstructural properties of ambient cured fly ash-based geopolymer mortar for onsite applications. *Results in Engineering*, 2023, 18, 101123. https://doi.org/10.1016/j.rineng.2023.101123

[33] Zhang, P. et al. High-temperature behavior of polyvinyl alcohol fiber-reinforced metakaolin/fly ash-based geopolymer mortar. *Composites Part B: Engineering*, 2022, 244, 110171. https://doi.org/10.1016/j.compositesb.2022.110171

[34] Zhong, Q.; Xie, G.; Nie, H.; Peng, H. Medium transmission property of the interfacial transition zone between MK-GGBFS geopolymer mortar and aggregate. *Construction and Building Materials*, 2024, 411, 134542. https://doi.org/10.1016/j.conbuildmat.2023.134542

[35] Kanagaraj, B. et al. Performance of Sustainable Insulated Wall Panels with Geopolymer Concrete. *Materials*, 2022, 15 (24), 8801. https://doi.org/10.3390/ma15248801
[36] Rout, M. K. D. et al. Feasibility Study of Reclaimed Asphalt Pavements (RAP) as Recycled Aggregates Used in Rigid Pavement Construction. *Materials*, 2023, 16 (4), 1504. https://doi.org/10.3390/ma16041504
[37] Rahman, S. S.; Khattak, M. J. Feasibility of Reclaimed Asphalt Pavement Geopolymer Concrete as a Pavement Construction Material. *International Journal of Pavement Research and Technology*, 2023, 16 (4), pp. 888-907. https://doi.org/10.1007/s42947-022-00169-8
[38] Rahman, S. S.; Khattak, M. J. Mechanical and Durability Characteristics of Roller Compacted Geopolymer Concrete Using Reclaimed Asphalt Pavement. In: *Proceedings of the International Conference on Civil Infrastructure and Construction (CIC 2020)*, Sirin, O. (ed.). February 2-5, 2020, Doha, Qatar, Qatar University Press; 2020, pp. 420-430. https://doi.org/10.29117/cic.2020.0053
[39] Ali, H.; Rojali, A. Recycling Asphalt Pavements: The State of Practice. In: *Recycling Strategy and Challenges Associated with Waste Management Towards Sustaining the World*, Saleh, H. M.; Hassan, A. I. (eds.). IntechOpen; 2023. https://doi.org/10.5772/intechopen.106235
[40] European Asphalt Pavement Association EAPA. Asphalt in Figure 2020. Accessed: May 5, 2025. Available at: https://eapa.org/press-release-asphalt-in-figures-2020/
[41] Singh, S.; Ransinchung, G. D. R. N.; Kumar, P. Feasibility study of RAP aggregates in cement concrete pavements. *Road Materials and Pavement Design*, 2019, 20 (1), pp. 151-170. https://doi.org/10.1080/14680629.2017.1380071
[42] Noor-ul-Amin; Faisal, M.; Muhammad, K.; gul, S. Synthesis and characterization of geopolymer from bagasse bottom ash, waste of sugar industries and naturally available china clay. *Journal of Cleaner Production*, 2016, 129, pp. 491-495. https://doi.org/10.1016/j.jclepro.2016.04.024
[43] Sales, A.; Lima, S. A. Use of Brazilian sugarcane bagasse ash in concrete as sand replacement. *Waste Management*, 2010, 30 (6), pp. 1114-1122. https://doi.org/10.1016/j.wasman.2010.01.026
[44] Akbar, A. et al. Sugarcane bagasse ash-based engineered geopolymer mortar incorporating propylene fibers. *Journal of Building Engineering*, 2021, 33, 101492. https://doi.org/10.1016/j.jobe.2020.101492
[45] Bayer Öztürk, Z.; Çam, T. Performance of eco-friendly fly ash-based geopolymer mortars with stone-cutting waste. *Materials Chemistry and Physics*, 2023, 307, 128112. https://doi.org/10.1016/j.matchemphys.2023.128112
[46] Saloma, H.; Pratiwi, K. I. Effect NaOH Concentration on Bagasse Ash Based Geopolymerization. *MATEC Web of Conferences*, 2016, 78, 01025. https://doi.org/10.1051/matecconf/20167801025
[47] El Abd, A. et al. Characteristics and neutron imaging of capillary water absorption for metakaolin and steel fiber reinforced slag based-geopolymer mortars. *Journal of Building Engineering*, 2024, 82, 107960. https://doi.org/10.1016/j.jobe.2023.107960
[48] Aredes, F. G. M. et al. Effect of cure temperature on the formation of metakaolinite-based geopolymer. *Ceramics International*, 2015, 41 (6), pp. 7302-7311. https://doi.org/10.1016/j.ceramint.2015.02.022
[49] Alhawat, M. et al. Properties of geopolymers sourced from construction and demolition waste: A review. *Journal of Building Engineering*, 2022, 50, 104104. https://doi.org/10.1016/j.jobe.2022.104104
[50] Bureau of Indian Standards. IS 1489 (Part 1). *Portland-Pozzolana cement-Specification: Fly Ash Based*. New Delhi: IS; 1993.
[51] Sharmila, S.; Natarajan, N.; Dineshkumar, S. Analysis of microstructural properties and durability characteristics of geopolymer mortar. *Materials Today: Proceedings*, 2023, 93 (Part 3), pp. 217-222. https://doi.org/10.1016/j.matpr.2023.07.138

[52] Sharmin, S. et al. Characterization of waste clay brick powder and its effect on the mechanical properties and microstructure of geopolymer mortar. *Construction and Building Materials*, 2024, 412, 134848. https://doi.org/10.1016/j.conbuildmat.2023.134848
[53] Nazir, K.; Canpolat, O.; Uysal, M. Durability properties of steel, polyamide, and polyethylene fiber-reinforced geopolymer mortar made with recycled concrete aggregate and glass powder as fillers. *Journal of Building Engineering*, 2023, 76, 107313. https://doi.org/10.1016/j.jobe.2023.107313
[54] Farag Gaddafi, A. K. et al. Enhancement of ductility characteristics of fiber-reinforced ternary geopolymer mortar. *Journal of Building Engineering*, 2024, 82, 108141. https://doi.org/10.1016/j.jobe.2023.108141
[55] Mashri, M. O. M.; Johari, M. A. M.; Ahmad, Z. A.; Mijarsh, M. J. A. Enhancing the properties of UPOFA-based geopolymer mortar via the incorporation of eggshell ash and silica fume. *Journal of Building Engineering*, 2023, 65, 105677. https://doi.org/10.1016/j.jobe.2022.105677
[56] Breiman, L. Random Forests. *Machine Learning*, 2001, 45, pp. 5-32. https://doi.org/10.1023/A:1010933404324
[57] Grömping, U. Variable Importance Assessment in Regression: Linear Regression versus Random Forest. *The American Statistician*, 2009, 63 (4), pp. 308-319. https://doi.org/10.1198/tast.2009.08199
[58] Otchere, D. A. et al. Application of gradient boosting regression model for the evaluation of feature selection techniques in improving reservoir characterisation predictions. *Journal of Petroleum Science and Engineering*, 2022, 208 (Part E), 109244. https://doi.org/10.1016/j.petrol.2021.109244
[59] Khan, M. I.; Abbas, Y. M. Robust extreme gradient boosting regression model for compressive strength prediction of blast furnace slag and fly ash concrete. *Materials Today Communications*, 2023, 35, 105793. https://doi.org/10.1016/j.mtcomm.2023.105793
[60] Parhi, S. K.; Patro, S. K. Prediction of compressive strength of geopolymer concrete using a hybrid ensemble of grey wolf optimized machine learning estimators. *Journal of Building Engineering*, 2023, 71, 106521. https://doi.org/10.1016/j.jobe.2023.106521
[61] Alwathaf, A. H.; Abdel Jaber, M.; Hunaiti, Y. M. Enhancement and Optimization of the Mechanical Properties in Cement Concrete with Recycled Asphalt Pavement (RAP). *Buildings*, 2024, 15 (1), 108. https://doi.org/10.3390/buildings15010108
[62] Singh, S.; Ransinchung, G. D.; Kumar, P. Effect of mineral admixtures on fresh, mechanical and durability properties of RAP inclusive concrete. *Construction and Building Materials*, 2017, 156, pp. 19-27. https://doi.org/10.1016/j.conbuildmat.2017.08.144
[63] Sarfaraz Ali, M.; Sachan, A. K. A review on the durability and applicability of Geopolymer concrete from the recent research studies. *Materials Today: Proceedings*, 2022, 52 (Part 3), pp. 911-922. https://doi.org/10.1016/j.matpr.2021.10.302
[64] Kurt, Z.; Yilmaz, Y.; Cakmak, T.; Ustabaş, I. A novel framework for strength prediction of geopolymer mortar: Renovative precursor effect. *Journal of Building Engineering*, 2023, 76, 107041. https://doi.org/10.1016/j.jobe.2023.107041
[65] Gopalakrishna, B.; Dinakar, P. Life cycle assessment (LCA) and the influence of alkaline activator content on mechanical and microstructural properties of geopolymer mortar. *Journal of Engineering Research*, 2024, In Press. https://doi.org/10.1016/j.jer.2024.01.010
[66] Srinivasa, A. S.; Yaragal, S. C.; Swaminathan, K.; Rakesh Kumar Reddy, R. Multi-objective optimization of one-part geopolymer mortars adopting response surface method. *Construction and Building Materials*, 2023, 409, 133772. https://doi.org/10.1016/j.conbuildmat.2023.133772

[67] Haily, E. et al. Use of a form-stable phase change material to improve thermal properties of phosphate sludge-based geopolymer mortar. *Construction and Building Materials*, 2023, 386, 131570. https://doi.org/10.1016/j.conbuildmat.2023.131570

[68] Zhang, H. et al. Compressive behaviour and microstructure of geopolymer mortar subjected to cryogenic freeze-thaw cycle: Effects of cycles and polypropylene fiber. *Cement and Concrete Composites*, 2024, 149, 105505. https://doi.org/10.1016/j.cemconcomp.2024.105505